Alvarez-Donado, R.; Papanikolaou, S.; Esfandiarpour, A.; Alava, M. J.

Viewing high entropy alloys through glasses: Linkages between solid solution and glass phases in multicomponent alloys

Published in:
Physical Review Materials

DOI:
10.1103/PhysRevMaterials.7.025603

Published: 01/02/2023

Document Version
Publisher's PDF, also known as Version of record

Please cite the original version:
Alvarez-Donado, R., Papanikolaou, S., Esfandiarpour, A., & Alava, M. J. (2023). Viewing high entropy alloys through glasses: Linkages between solid solution and glass phases in multicomponent alloys. *Physical Review Materials*, *7*(2), 1-9. Article 025603. https://doi.org/10.1103/PhysRevMaterials.7.025603

Viewing high entropy alloys through glasses: Linkages between solid solution and glass phases in multicomponent alloys

R. Alvarez-Donado,[1] S. Papanikolaou,[1] A. Esfandiarpour,[1] and M. J. Alava[1,2]
[1]*NOMATEN Centre of Excellence, National Centre for Nuclear Research, ul. A. Soltana 7, 05-400 Swierk/Otwock, Poland*
[2]*Aalto University, Department of Applied Physics, PO Box 11000, 00076 Aalto, Finland*

(Received 30 March 2022; accepted 3 February 2023; published 23 February 2023)

High entropy alloys (HEAs) represent highly promising multicomponent crystals that form concentrated solid solutions (CSSs) and may violate traditional thermodynamic rules of mixing, ultimately leading to excellent physical properties. For a deeper understanding, we investigate seven CSSs, including Co-Cr-Ni-Fe-Mn elements, at experimentally relevant compositions and conditions, through molecular simulations, and we use 1-1 comparisons to corresponding glass state characteristics, attained through rapid cooling protocols. We determine the behavior of various structural features, including the configurational entropy for a set of CSSs in their crystalline and vitreous states numerically. We employ swap Monte Carlo (MC) simulations, in combination with the reversible scaling method, to efficiently compute the configurational entropy ($S_{\rm conf}$), and show that the entropic rule of mixing is not always adequate for predicting alloy formation. We study the stability and formability of crystalline solid solutions, as well as glasses, while following the thermodynamics of $S_{\rm conf}$. An apparent entropic similarity between CSSs and corresponding glasses leads us to use a Kauzmann-like ansatz, relating the CSSs at $S_{\rm conf} \to 0$ with the emergence of a CSS order-disorder transition, at temperature T_{OD}. In the context of glasses, a comparison between kinetic and thermodynamic fragilities allows the association of sluggish diffusion onset to a drop in $S_{\rm conf}$ at T_K. Analogously, we classify CSSs as *"strong"* or *"fragile"* in the sense of their ability to migrate across CSS crystal configurations at high temperatures, distinguishing its formability. We argue that the magnitude of T_{OD} may be an excellent predictor of CSS single-phase stability, which appears to scale with well-known HEA predictors, in particular we notice that VEC and T_{OD} have in relation to the others a significantly large Pearson correlation coefficient, much larger than most other observables (except $\Delta H_{\rm mix}$).

DOI: 10.1103/PhysRevMaterials.7.025603

I. INTRODUCTION

The synthesis of random single-crystal phase alloys containing equiatomic or near equiatomic concentration, the so-called concentrated solid solutions (CSSs), has opened the door for a completely new kind of material with outstanding properties [1–8], such as hardness values from 1.27 to 10.79 GPa [9], corrosion resistance as good as stainless steel, and excellent oxidation resistance, up to 1400 K [10]. The stability of these CSSs were originally associated with a design strategy, which benefits the maximization of the configurational entropy, $S_{\rm conf}$. Notwithstanding, this strategy has led to successful random single solid solutions only in a reduced number of compositions [11–13], where the role of $S_{\rm conf}$ is still unclear [14,15]; moreover, nonequiatomic compositions have proven to be more stable under similar conditions [16–20]. Thus, the validity of $S_{\rm conf}$ to determine stability in CSSs, as well as the question of whether better predictors of CSS stability exist are still debated topics [21,22].

In contrast, amorphous metallic solids, also known as metallic glasses (MGs), have been studied since the second half of the 1990s [23], and commonly exhibit unusual properties, such as remarkable mechanical strength and stiffness, thermoplastic forming, high restitution coefficient, and soft magnetic properties [24–26]. In this framework, the configurational entropy is associated with the number of minima of the system's energy landscape [27]. Thus, the viscous slowing down appearing in the supercooled liquid when the temperature approaches that of the glass transition (T_g) is a consequence of the decrease in the number of configurations that the system is available to sample. This interpretation is the basis of the Adam-Gibbs (AG) equation [28], a mathematical expression that gives an exponential relation between $S_{\rm conf}$ and kinetic properties (such as the self-diffusion coefficient [29,30], the relaxation time [31,32], or the viscosity [28,33]) providing an explanation of the dynamic behavior in thermodynamic terms.

MGs and CSSs have been synthesized based on three similar design criteria. First, the number of species, usually three or more with one of them as a principal element in MGs and equiatomic composition in the case of CSSs. Second, the atomic mismatching, up to 12% in MGs and the atomic size difference δ in CSS, and third, combination of thermochemical parameters such as entropy of mixing ($\Delta S_{\rm mix}$), melting points (T_m), the enthalpy of mixing ($\Delta H_{\rm mix}$), or valence electron concentration (VEC). However, these empirical criteria have a number of limitations, the most pronounced of which is that temperature plays an important role to determine phase stabilities of solution phases, but most of these parameters do not consider the effect of temperature. Here,

physically motivated and novel criterion, based on extensive investigations of thermomechanical aspects of CSSs in various compositions. We compute numerically the configurational entropy of a quinary $Co_{20}Cr_{20}Ni_{20}Fe_{20}Mn_{20}$ alloy, as known as Cantor alloy [12], as well as seven variants of this alloy. We chose the aforementioned alloys for three main reasons: (i) CSSs based on the Cantor alloy have been systematically used to explore the properties of CSSs [12–14,22,34–38], (ii) the possibility to obtain these samples experimentally in the glass state through the electrosynthesis of salts [37], and (iii) to apply our methodology to real systems. Our results allow us to establish a relation between the sluggish diffusion in solid solutions with the drop in the configurational entropy in an analogous manner as occurs in the glassy systems. Using the glass ansatz equation for the configurational entropy in our results for the CSS we determine the order-disorder transition temperature in solid solutions, T_{OD}, and then we show that T_{OD} appears to scale with well-known HEA predictors, in particular we notice that VEC and T_{OD} have a noticeable Pearson correlation coefficient. In this way, we propose that T_{OD} may be an appropriate predictor of phase stability in HEAs.

In this paper, by using molecular-dynamics simulations of multicomponent alloys, we develop an analogy between CSSs and glasses, by identifying an apparent CSS order-disorder transition temperature T_{OD} as an excellent predictor of CSS thermomechanical stability. A key behind thermomechanical stability is rooted in the connection of thermodynamically accessible configuration dynamics. In particular, the dramatic slowing down in supercooled liquids might be explained in entropy terms [30], and possibly analogies may be extracted for the behavior of CSSs and HEAs.

The reminder of the paper is organized as follows: In Sec. II we present the simulation setups employed to generate the glass and solid solution structures. Section III describes the methodology we used in order to compute the configurational entropy. In Sec. IV we discuss our results, particularly the order-disorder transition in solid solutions and the similarity in the behavior of the configurational entropy in the "orthogonal" crystal and amorphous states. Finally, Sec. V summarizes our conclusions and future perspectives of this work.

II. SIMULATION SETUP

The interatomic interactions for the Co-Cr-Fe-Ni-Mn-based alloys are described by a second-nearest neighbor modified embedded atom method (2NN-MEAM) [39] provided in Ref. [40]. We simulate different element alloy combinations in equiatomic compositions of these elements. Excluding the five-element alloy (for which $N = 6000$), the simulation cell consists of $N = 6336$ atoms in a cubic box with periodic boundary conditions (PBCs) in all three dimensions. Our simulations were carried out in the molecular-dynamics (MD) open code LAMMPS [41], using a time step $\Delta t = 1$ fs. To begin with, we define an initial face-centered cubic (fcc) supercell to be filled with randomly distributed atoms. Once the initial structure was created we equilibrated it at $T = 300$ K during 2 ns. The glass state was obtained through the melting of the crystalline structure, heating the system from 300 to 2800 K and after doing a quenching using a cooling rate $\kappa = 100$ K/*ns*. We saved configurations every 50 K during the heating and cooling processes. Each of the aforementioned configurations were equilibrated for 1 ns in order to obtain the dynamic and thermodynamic properties. The heating and cooling processes were performed by integrating the Nosé-Hoover equations [42,43] with damping parameters $\tau_T = 2$ fs and $\tau_p = 5$ ps for the thermostat and barostat, respectively. All results were obtained keeping the external pressure $p = 0$. The equilibrated samples were changed to the NVT ensemble and the simulation box was rescaled to the average equilibrium volume in the NpT ensemble which gives an external pressure $p = 0$. Finally, for the Monte Carlo (MC) swaps, we randomly choose two different particles with different types and we estimate the energy cost to exchange them [44]. The moves are accepted according to the usual Metropolis criterion, guaranteeing detailed balance.

III. PROTOCOL AND METHODS

A. Reversible scaling

We have numerically computed the entropy (S) of the system through its free energy (G). Since both variables depend on the entire volume of the phase space, standard MC or MD simulations cannot be used to measure them and special methods are necessary. Here, we have employed the reversible scaling (RS) method, which is based on the creation of a specific path defined by a scaling factor $\zeta(t)$ in the potential energy of the interest system [45]. For the case of the 2NN-MEAM we have $U_{\text{scaled}} = \zeta(t) U_{\text{MEAM}}$ and the free energy is determined using the RS formula [45–47]

$$G(T) = \frac{G_{\text{MEAM}}(T_0)}{\zeta(t)} + \frac{3}{2} N k_B T_0 \frac{\ln \zeta(t)}{\zeta(t)} + \frac{\mathcal{W}(t)}{\zeta(t)}, \quad (1)$$

where $G_{\text{MEAM}}(T_0)$ is the free energy of the system at a specific reference temperature T_0, T is the final temperature defined by $T = T_0/\zeta(t)$, and

$$\mathcal{W}(t) = \int_0^{t_s} d\tau \left. \frac{d\zeta}{d\tau} \right|_t U_{\text{MEAM}}(R(\tau)) \quad (2)$$

is the irreversible work done to bring the system from T_0 to T, and $R(t)$ is a vector containing the position of all the atoms at the instant t.

This method offers the advantage to provide the free energy $G(T)$ in a wide range of temperatures by performing only one (MD or MC) simulation. However, two conditions should be met in order to apply the RS method. First, $G_{\text{MEAM}}(T_0)$ has to be known beforehand and, second, the dissipative error generated by the dynamic work must be eliminated by a hysteresis process [47]. Computing $G_{\text{MEAM}}(T_0)$ will depend on the specific state of the system of interest, for the glass and the solid solution the details are presented in the next sections. Here we focus on how to determine $\mathcal{W}(t)$. Equation (1) express the fact that computing $G(T)$ is equivalent to the problem of computing the irreversible work in Eq. (2) when the parameter $\zeta(t)$ varies from T_0 to $T = T_0/\zeta(t)$. In general the functional form of $\zeta(t)$ is to be chosen wisely to reduce the dissipative error generated by the nonequilibrium process. Notwithstanding, for glasses ζ cannot vary arbitrarily during the simulation in order to keep a fix cooling rate. Thus,

to find a temporal-functional form to ζ that preserves the cooling rate constant we impose the condition:

$$\frac{dT}{dt} = \kappa, \tag{3}$$

where κ is the cooling rate at which the system will be quenched.

Remembering that the temperature in the RS method is given by $T = T_0/\zeta$, we have $dT = d(T_0/\zeta)$, and Eq. (3) can be integrated to obtain

$$\zeta(t) = \frac{T_0}{T_0 + \kappa t}. \tag{4}$$

The initial temperature T_0 we chose as $T_0 = 300$ K and the cooling rate κ is positive and negative for the crystal and liquid, respectively. Since we are interested in calculate the free energy in the supercooled regime (between [1000–1500] K) we have

$$1500\ \text{K} = \frac{300\ \text{K}}{\zeta}.$$

Then ζ will temporally evolve from 1 to 0.2 according to Eq. (4). Finally, $\mathcal{W}(t)$ is computed using Eq. (2). The integration involves instantaneous values of $\frac{d\zeta(t)}{dt}U_{\text{MEAM}}$. Therefore, the work performed during the scaling is irreversible in nature and provides two types of errors that originate in simulation limitations: First, a statistical error associated with the fact that the integral of Eq. (2) depends on the initial conditions of the irreversible process, due to the practical presence of a finite upper time limit. Second, a systematic error arises from the dissipative entropy production generated by the non-quasistatic change of parameters during the integration. This entropy production causes that the mean of the irreversible work distribution shifts with respect to the value of the ideal quasistatic work W_{qs}. Since in simulations, we cannot deal with infinite times, these two errors naturally appear in our calculations. Fortunately, in practice, the convergence of the finite width distribution to the ideal one is remarkably fast [45] and standard simulations with length comparable to typical equilibrium MC or MD simulation are enough to considerably reduce both errors. Moreover, if the simulations are performed slow enough to guarantee the validity of the linear response, the energy dissipation will be the same if we perform the driving process from $T_0 \to T$ or from $T \to T_0$ [47]. Thus, the quasistatic work and the dissipative energy can be estimated by

$$\begin{aligned} W_{qs} &= \frac{\langle \mathcal{W} \rangle^{T_0 \to T} - \langle \mathcal{W} \rangle^{T \to T_0}}{2}, \\ \Delta E_{\text{diss}} &= \frac{\langle \mathcal{W} \rangle^{T_0 \to T} + \langle \mathcal{W} \rangle^{T \to T_0}}{2}, \end{aligned} \tag{5}$$

where $\langle \cdot \rangle$ represents a mean of independent initial configurations.

This strategy is always applicable if the system does not undergo a phase transition and the path $T_0 \to T$ leads to identical work (in absolute terms) as $T \to T_0$.

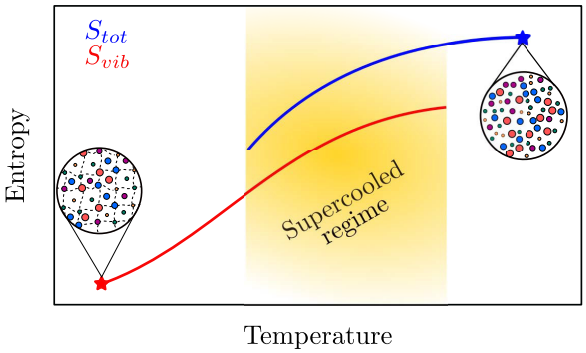

FIG. 1. Schematic representation of the calculation of S_{tot} and S_{vib} using the RS method. $G_{\text{MEAM}}(T_0)$ is represented by the red and blue stars for solid and liquid phase, respectively. The yellow region is the supercooled regime where $S^g_{\text{conf}} = S_{\text{tot}} - S_{\text{vib}}$.

B. Configurational entropy I: Glass state

The configurational entropy in the glass state (S^g_{conf}) is obtained by applying the definition [29,48,49] where S_{tot} is the total entropy and S_{vib} is the thermal vibrational contribution computed in the neighborhood of a reference configuration [50,51]. These quantities are obtained from the free energy using the thermodynamic relation

$$S_\alpha = \frac{G_\alpha - H_\alpha}{T}, \tag{6}$$

where $\alpha =$ vib, tot stands for vibrational or total, and H and T are the enthalpy and the absolute temperature, respectively.

To apply the RS method to compute the free energy, we have to determine the reference free energy $G_{\text{MEAM}}(T_0)$ in the solid and liquid phase. This is done by thermodynamic integration or adiabatic switching choosing wisely the reference system. We use the Einstein crystal (collection of harmonic oscillators) and the Uhlenbeck-Ford model (UFM) [52,53] as reference system in the glass and liquid state, respectively. It is important to note that these reference systems are only used to determine the reference free energies at low temperature, ($T_0 = 300$ K) for S_{vib} [50,51,54,55] and high temperature ($T_0 = 2300$ K) for S_{tot} [52,53,56]. We only measure S^g_{conf} in the supercooled regime where we can separate S_{tot} in $S_{\text{vib}} + S_{\text{conf}}$.

Figure 1 shows a schematic representation of the numerical computation of S_{tot} and S_{vib} through the RS method. In the crystalline solid phase G^0_{MEAM} (red star in Fig. 1) the atoms are fixed in the lattice structure and they can only move around its equilibrium position. Thus, only the vibrational degrees of freedom are taking into account during the computation. In the liquid phase, on the other hand, G^0_{MEAM} (blue star in Fig. 1) contains information on vibrational and configurational contributions since atoms are free to move. In the supercooled regime (yellow region in Fig. 1) the configurational entropy is obtained as $S^g_{\text{conf}} = S_{\text{tot}} - S_{\text{vib}}$.

C. Configurational entropy II: Solid solution

Computing the configurational entropy for a solid solution (S^{SS}_{conf}) requires preserving the lattice structure and allow the atoms to explore different configurations simultaneously. This

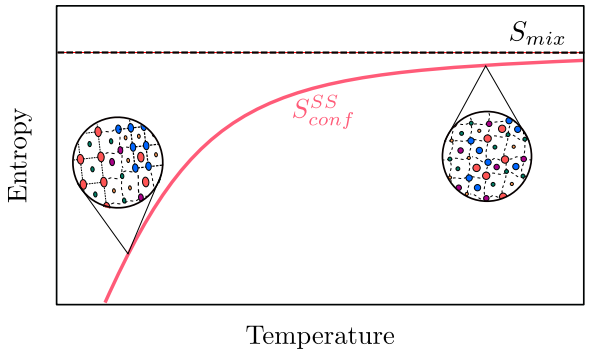

FIG. 2. Schematic representation of the calculation of the configurational entropy in the solid solution phase. At high temperatures $S^{SS}_{\rm conf} = S_{\rm mix}$ (dashed black line). However, when the temperature is below T_m, $S^{SS}_{\rm conf}$ deviates from the ideal value due to segregation or precipitation.

kind of calculation cannot be performed using MD simulations where the atoms in a solid are fixed and they move only around their equilibrium position. Therefore, to compute $S^{SS}_{\rm conf}$ we employ the MC swap method. To do so, we set a fcc crystalline structure at fixed volume corresponding to the equilibrium volume obtained at $T = 900$ K and $p = 0$ bars. Then we perform a series of MC swaps consisting in randomly choosing two atoms and exchanging their types. The moves are accepted or rejected according the Metropolis criterion, guaranteeing the detailed balance. Since the MC swaps only involve redistribution of the atomic population, the lattice structure is preserved for any temperature. Because the system remains crystalline even when $T \to \infty$, thus we can use as the reference free energy $G_{\rm MEAM}(T_0 = \infty) = -TS_{\rm mix}$. This highlights another of the advantages of use the RS method, we can map the problem of determining free energy for an infinite interval of temperature onto a problem of finding the free energy for a finite interval of the scaling parameter $\zeta(t)$. The logarithmic term in Eq. (1) corresponds to the kinetic degrees of freedom, and must be omitted when we calculate $S_{\rm conf}$ for the SS ($S^{SS}_{\rm conf}$) since only configurational changes are considered. In Fig. 2, we present a schematic representation of the temperature evolution of $S^{SS}_{\rm conf}$ obtained by means of RS method performing MC swaps. The deviation in the ideal $S_{\rm mix}$ is associated with a degree of order in the solid solution due to segregation, precipitation or spinodal decomposition.

IV. PHASE STABILITY OF THE CANTOR ALLOY

Let us focus first on the thermodynamic evolution of the Cantor alloy during a heating and cooling process. Figure 3(a) shows the volume evolution as a function of temperature between 300 and 2500 K. During the heating process (red points) we found the mechanical stability limit of the fcc structure being $T^{\rm mech}_m = 1900$ K at the Lindemann's parameter $\delta = 0.12$. The Cantor alloy does not present volume discontinuity by quenching the liquid (blue points), and the glass transition temperature,$T_g = 1050$ K was determined by using the Kuwabcheski relations [57] in the same way as in Refs. [58,59]. The thermodynamic melting point (T_m) is given by the temperature at which the liquid ($G_{\rm tot}$) and crystalline ($G_{\rm vib}$) phase have the same free energy [Fig. 3(b)]. We determined the crossing temperature to be $T_m = 1470$ K. This value even being 5% lower from the experimental one, $T^{\rm exp}_m = 1553$ K obtained by Wu *et al.* [60] by differential scanning calorimetry is still quite accurate and we use it as a first test of the validation of our results. Figure 3(c) depicts the crystalline and liquid entropy as a function of temperature obtained by means of $G_{\rm vib}$ and $G_{\rm tot}$, respectively. Again the computed values are in a good agreement with the experimental data [61] [black line in Fig. 3(c)], providing our second validation test. Since during our simulations we used PBC the system is allowed to be superheated ($T^{\rm mech}_m > T_m$) and the temperature windows to which we are able to measure $S_{\rm conf}$ is higher than in experimental procedures. Thus, we define our supercooled regime between $T^{\rm mech}_m$ and T_g [yellow region in Figs. 3(a) and 3(c)]. Figure 3(d) shows the $S^g_{\rm conf}$ as a function of temperature in the supercooled regime. For values below T_g the value of $S^g_{\rm conf}$ becomes almost constant starting the nonequilibrium glass regime. Here, we focused in the (meta)equilibrium behavior therefore, we did not include values below T_g.

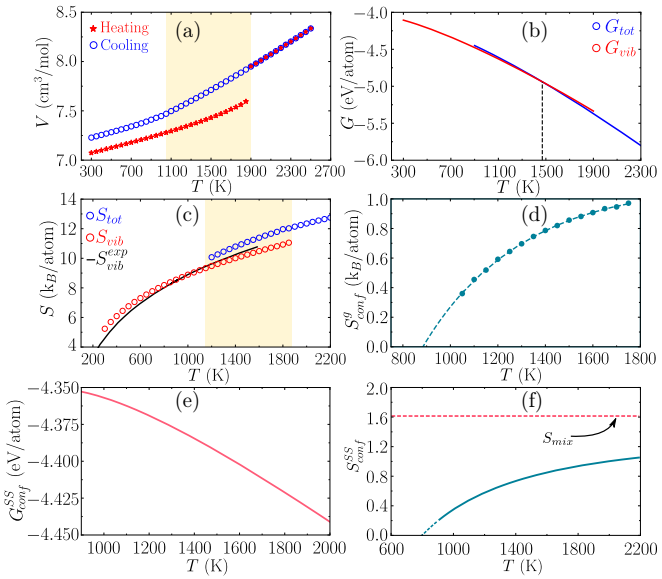

FIG. 3. Thermodynamic properties of the $Co_{20}Cr_{20}Ni_{20}Fe_{20}Mn_{20}$ Cantor alloy (a) Volume as a function of the temperature during the heating (red) and quenching (blue) processes. (b) Absolute Gibbs free energy for the solid (red) and the liquid (blue) phases. The thermodynamic melting point is obtained as the crossing between $G_{\rm tot}$ and $G_{\rm vib}$. (c) Entropy as a function of temperature obtained by means of the respective free energy. The values of $S^{\rm exp}_{\rm vib}$ were taken from the experimental measures reported in Ref. [61]. (d) Temperature evolution of $S^g_{\rm conf}$ in the supercooled regime [yellow region in panels (a) and (c)]. The dashed line are obtained by fitting the computed data (see main text). (e), (f) Configurational free energy and entropy for the solid solution and their temperature dependence. Even at high temperatures $S^{SS}_{\rm conf}$ is far form the ideal $S_{\rm mix}$ value.

The entropy crisis predicted by Kauzmann happens when $S^g_{\rm conf} = 0$ for $T > 0$. Since we do not compute $S^g_{\rm conf}$ below T_g, we fit our data according to [32,62,63]

$$TS^g_{\rm conf} = A(T - T_K) + B(T - T_K)^2, \tag{7}$$

TABLE I. Relevant temperatures during the cooling and heating of the alloys. Experimental melting temperatures (T_m^{expt}), 2NN-MEAM melting temperature (T_m), glass transition temperature (T_g), Kauzmann temperature (T_K), and order-disorder temperature (T_{OD}).

Alloy	T_m^{expt} (K)	T_m (K)	T_g (K)	T_K (K)	T_{OD} (K)
CoCrNiFeMn	1553	1470	1050	886	799
CoCrNiMn	1489	1465	950	768	605
CoCrNiFe	1695	1730	1150	949	681
CoNiFe	1724	1740	1050	831	770
FeNiMn	1473	1500	900	768	612
FeNiCr		1690	1150	1000	712
FeNi	1703	1670	1150	904	818

where A and B are associated with the thermodynamic fragility and T_K is the so-called Kauzmann temperature—a temperature to which the liquid experience an ideal glass of unique configuration resulting in a zero configurational entropy. This fitting function allows us extrapolate our results to deeply supercooled states and estimate the thermodynamic glass transition at T_K.

The temperature evolution of the configurational entropy in the CSS is shown in Fig. 3(f). S_{conf}^{SS} was obtained in this case by computing numerically $\partial\langle G_{\text{conf}}^{SS}\rangle/\partial T$ where $\langle\cdot\rangle$ denotes a mean value over uncorrelated samples of the configurational free energy [Fig. 3(e)]. From the evolution of S_{conf}^{SS} we notice that, first, S_{conf}^{SS} tends to deviates from the ideal S_{mix} [dashed line in Fig. 3(f)], even at very high temperatures—higher than the melting point. As such, the value of S_{mix} is just an upper limit difficult to reach in practice [22,64], and second, the behavior of S_{conf}^{SS} as a function of the temperature is similar to the one obtained for the glass state [Fig. 3(d)]. The overall trend of S_{conf}^{SS} is similar to those computed in recent studies of CSS based on the cluster-variation method [22,64–66]. For temperatures below 900 K the simulation time required to keep the system in equilibrium exceeds our current computational resources. Therefore, motivated for the similarity temperature dependence of S_{conf} in the CSS and glass states, we extrapolated our data from S_{conf}^{SS} using the same fitting equation that we employed for the glass state. However, in this case we associate the T_K parameter—associated with a unique glass configuration—with an order-disorder transition temperature T_{OD} at which short-range order appears in the CSS alloy. We note in passing that such a Kauzmann-like ansatz works well. Thus, when $T < T_{OD}$ the solid solution is not random anymore and as a consequence, e.g., some segregation, precipitation, or spinodal decomposition should appear in the system.

V. ORDER-DISORDER TRANSITIONS

We extend our study for a subset of Cantor CSSs in which quenching the liquid leads to a glassy state. For each alloy we compute the thermodynamic melting point T_m, the glass transition temperature T_g, the Kauzmann temperature in the glass state T_K, and the order-disorder transition temperature T_{OD} for their CSS counterpart. These temperatures are summarized in Table I .

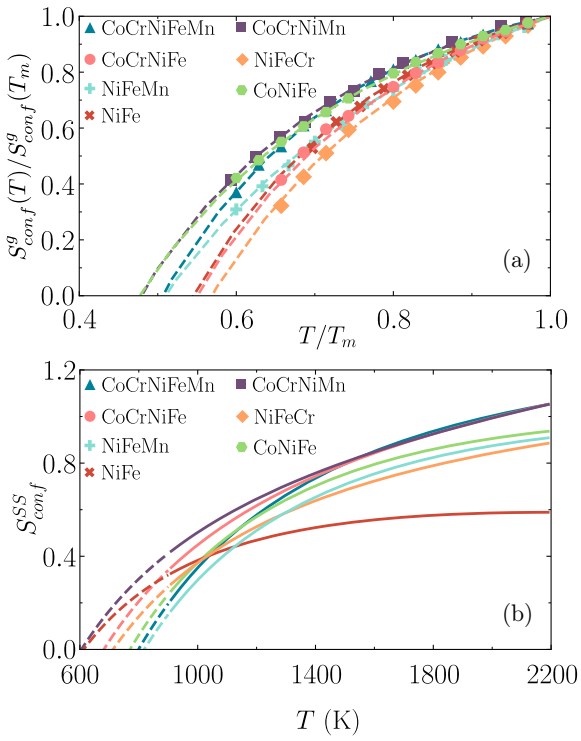

FIG. 4. Temperature dependence of configurational entropy for a subset of Cantor alloys (a) Kauzmann plot of the glass configurational entropy as a function of T. Both axes are normalized by the thermodynamic melting temperature T_m. The extrapolation to lower temperatures suggest a ideal glass transition with $S_{\text{conf}}^{g} = 0$. (b) Kauzmann-like plot of S_{conf}^{SS} as a function of temperature for the same set of alloys in the crystalline phase. The extrapolation to lower temperatures was obtained using the same fitting equation as for S_{conf}^{g}, we associate the vanishing in S_{conf}^{SS} with the order-disorder transition.

Figure 4(a) shows the so-called Kauzmann plot for all the glasses that we obtain, i.e., S_{conf}^{g} normalized by its value at T_m as a function of the normalized temperature T/T_m. The solid lines were obtained by fitting the values of S_{conf}^{g} with Eq. (7). The Kauzmann temperature of these alloys is in the interval [1000–760] K. In the same spirit of a Kauzmann-like plot in Fig. 4(b) we present S_{conf}^{SS} of these alloys normalized by their value at T_m as a function of the normalized temperature T/T_m and once more we fit the data using Eq. (7), but identifying T_K as the order-disorder transition temperature T_{OD}. With the value of T_{OD} we are capable to define a stability temperature limit of the random solid, i.e., for $T < T_{OD}$ the random solid solution decomposes in more ordered phases regardless of the number of components. Thus we are capable of determine the thermodynamic stability of the crystalline random solid solutions based on the similar behavior of S_{conf} in the CSS and glass states.

To demonstrate the validity of our approach we estimate the T_{OD} explicitly in a binary FeNi CSS by computing the short-range-order (SRO) parameter α and the configurational enthalpy H_{conf} when the system is annealed at different temperatures. To do so, we set a CSS of NiFe consisting of $N = 500$ atoms corresponding to the equilibrium volume obtained at $p = 0$ bars and $T = 300$ K. Then we perform a series of MC cycles, when every cycle consists of $N/2 = 250$ attempts

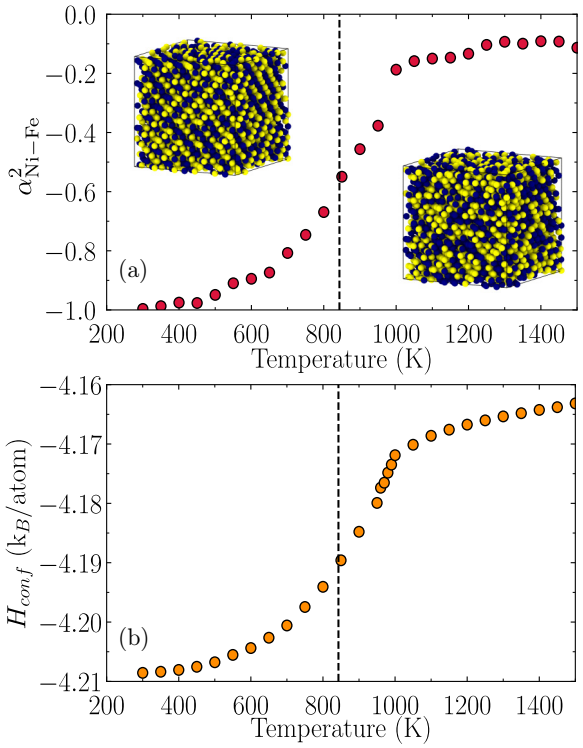

FIG. 5. (a) Pairwise short-range order parameter α_2 at different annealing temperatures. (b) Configurational enthalpy obtained by pure MC swaps at different temperatures. The order-disorder transition is represented by the dashed black line in the plot.

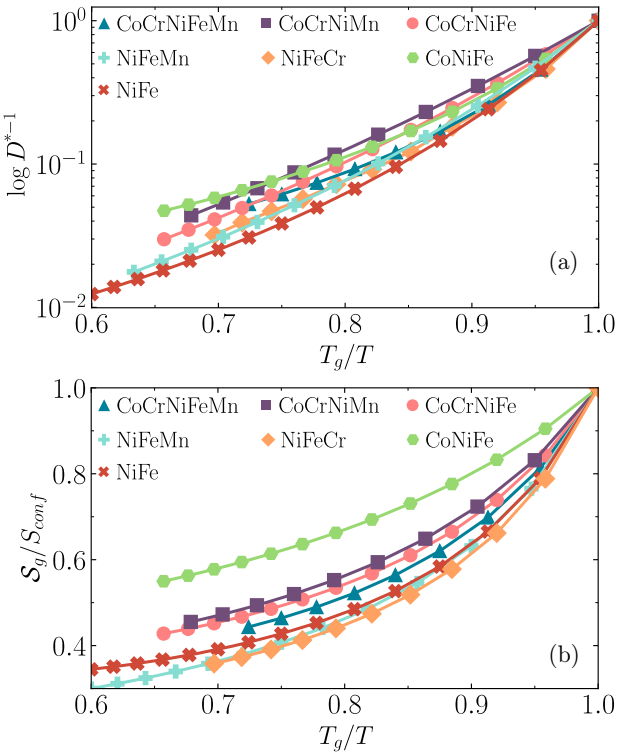

FIG. 6. (a) Kinetic Angell plot of the self-diffusion coefficient D against the reduced temperature T_g/T for seven Co-Cr-Fe-Ni-Mn based MPEAs. we normalize the D for its value at T_g to ease comparison between the alloys. (b) Thermodynamic Angell plot of the reduced configurational entropy $\mathcal{S}_g/S^g_{\rm conf}$ as a function of T_g/T. Here $\mathcal{S}_g$ stands for $S^g_{\rm conf}(T = T_g)$.

of exchanges. We perform a series of MC cycles (8×10^5 for $T < 1000$ K and 8×10^5 for $T \geqslant 1000$) on a relatively fine grid over a temperature interval of 1200 K. The SRO parameter was computed by [22]

$$\alpha^n_{ij} = 1 - \frac{P^n_{ij}}{C_j}, \tag{8}$$

where n means the nth-nearest-neighbor shell of the central atom i, P_{ij} is the average probability of finding a j-type atom around an i-type atom in the nth shell, C_j is the average concentration of j-type atom in the system.

Figure 5 shows the measured configurational enthalpy and the second-nearest neighbor SRO parameter for Ni-Fe pair. The abrupt change in both $H_{\rm conf}$ and α^2_{Ni-Fe} indicate an order-disorder transition occurring in the system. We estimate a $T_{OD} = 830$ K as the temperature at which $\partial H_{\rm conf}/\partial T$ presents a discontinuity (vertical black line in Fig. 5). To verify the volume effect, we perform an analogous calculation but using an equilibrium configuration corresponding to the equilibrium volume at $T = 0$ K, which yields a smaller volume than the one at $T = 300$ K. The resulting T_{OD} is just 2% larger than the one measured at $T = 300$ K, thus we conclude that the chosen value for the volume is irrelevant to our conclusions. The measured SRO parameter computed by this method is in good agreement with the one we previously obtained using the glass ansatz equation. Therefore, we conclude that our approach can be used to determine T_{OD} in CSS.

VI. KINETIC AND THERMODYNAMIC FRAGILITIES

Turning to the glass state, we explore the relation between the dynamics and thermodynamics of these alloys during cooling by means of their fragilities. To begin with, we calculate the mean squared displacement defined as

$$\Delta(t) = \langle |r_i(t) - r_i(0)|^2 \rangle, \tag{9}$$

where r_i is the position of the particle i at time t. The diffusion coefficient D is obtained from the Einstein relation: $D = \lim_{t\to\infty} \Delta(t)/6t$. The simulation is performed at sufficiently large t to reach the diffusion regime. The kinetic fragility is obtained from its definition as

$$m_k = \left.\frac{\partial \log D^{-1}}{\partial\left(T_g/T\right)}\right|_{T=T_g}. \tag{10}$$

The thermodynamic fragility, on the other hand, is given by

$$m_t = \left.\frac{\partial\left(S^g_{\rm conf}\right)^{-1}}{\partial\left(T_g/T\right)}\right|_{T=T_g}. \tag{11}$$

Figure 6 depicts Angell plots for both D [Fig. 6(a)] and $S^g_{\rm conf}$ [Fig. 6(b)], normalized by their values at T_g. We normalize $D^* = D/D(T_g)$ to account the shift in the values at T_g and to ease the comparison between systems. The kinetic (m_k) and thermodynamic (m_t) fragilities decreases faster than linearly (strong), presenting a super-Arrhenius (fragile) behavior. The

two fragilities m_k and m_t present a pretty similar values—between 14 and 26—and behavior with the exceptions of CoNiFe and NiFeCr. However, this difference has already been reported by Richet [67,68] and seems to result from the fact that the vibrational entropy of glass state is lower than that of the SS. Nonetheless, several results pointed out that the dramatic drops in $S_{\rm conf}$ are related with the decreasing of the configurational entropy and therefore the thermodynamic fragility [30,69,70]. The drops in entropy reduce the kinetic pathways and lead to the dramatic slowdown in the dynamics. From the similarities in the behavior of the two fragilities we can associate the slowing in the diffusion (kinetics) with a reduction in the number of accessible glass state that the system can reach, and therefore, the diminution in $S^g_{\rm conf}$ (thermodynamics). Based on the thermal evolution of $S^g_{\rm conf}$ and $S^{SS}_{\rm conf}$, we can classify CSSs as *strong* or *fragile* in the sense of their ability to migrate across the solid solution configurations at high temperatures. Thus, we can use a *fragile-strong* criterion for the stability of CSS, mainly arguing that when the entropy drop is faster so the stability of the random solid solution is reduced. Moreover, since in glass the kinetic and thermodynamic properties are related, we suggest that the diffusion in these CSSs should be similar to the glasses influenced by T as suggested by the temperature dependence of $S^{SS}_{\rm conf}$ and the Kauzmann-like fit in $S^g_{\rm conf}$. This is because both configurational entropies measure the number of accessible configurations ($\mathcal{N}$) in the system, but with $S^{SS}_{\rm conf}$ restricted at specific position in the lattice. In other words, the thermodynamic properties of SS could be related with kinetics as is in glasses. Thus, a thermodynamic-kinetic relation in CSS would provide an explanation for some open questions in the HEA community as the sluggish diffusion in HEA, or a vanishing configurational entropy in CSS at finite temperature. For the first case, experiments [71–73] and simulations [40,74] have shown that CoCrNiFeMn presents a slower diffusion than Fe-Ni-Cr alloys at equal homologous temperature. As we can see in Figs. 6(a) and 6(b), the NiFeCr, NiFeMn, and NiFe present a fragility index higher than CoCrNiFeMn resulting in a smaller drop in $S^g_{\rm conf}$, reducing the kinetic pathway, and leading to a slower diffusion. Moreover, among the five elements Co and Ni have the slower diffusion [40], thus the alloys that contain these two elements present as expected a slower diffusion.

Figure 7 depicts the values of the normalized (with respect to their respective maximum value) T_{OD} compared with other usual HEA predictors as VEC, δ, $\Delta H_{\rm mix}$ and the shear modulus mismatch (δ_G). We also included the Pearson correlation coefficient (ρ) for all observables in relation with T_{OD} and we notice that VEC and T_{OD} have a significantly large $\rho > 0$ (0.5) compared with most other observables (except $\Delta H_{\rm mix}$). This promotes future work on the possibility that T_{OD} can function of an effective predictor of stable HEA phases.

Retrospectively, recent simulation results based on MC simulations have shown a disorder-to-order transition when the annealing temperature decreases, suggesting an *"ideal"* SS structure for CSS. This transition might be related with spinodal decomposition or the appearing of more ordered phases due to segregation or precipitation of some elements in the alloy [75]. Two typical example of this phenomenon were reported by Li *et al.* in a ternary CoCrNi and Santodonato *et al.*

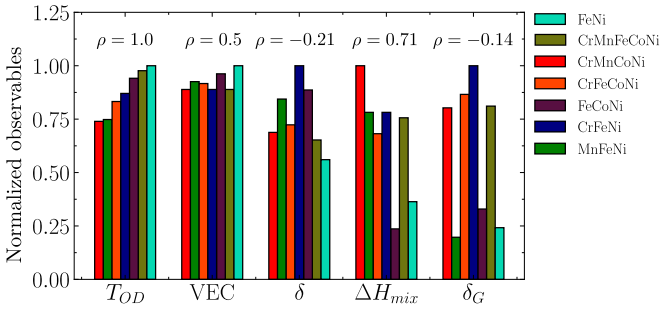

FIG. 7. Normalized values of the order-disorder transition (T_{OD}), valence electron concentration (VEC), atomic size mismatch (δ), enthalpy of mixing (ΔH), shear modulus mismatch (δ_G), and the Pearson correlation coefficient (ρ) in relation to T_{OD}.

[5] in a quinary CoCrNiFeAl HEA having this disorder-order transition approximately at 650 and 800 K, respectively, and coinciding with the vanishing values at T_{OD} that we obtain for similar alloys (see Table I).

VII. CONCLUSIONS AND PERSPECTIVES

We have presented a systematic study of the configurational entropy evolution during a heating and cooling processes for several multicomponent alloys in glassy and solid solution states and possible analogies that may be extracted between glassy and CSS phases. Our methodology reproduces well the thermodynamic melting point experimentally reported for these alloys, ensuring that the 2NN-MEAM potential describes well the interatomic interactions. We report a comparison of the temperature dependence of the configurational entropy in multicomponent alloys in crystalline and vitreous states, as well as the deviation of $S^{SS}_{\rm conf}$ from the ideal $S_{\rm mix}$ based on purely thermodynamic approaches. The difference between $S_{\rm mix}$ and $S^{SS}_{\rm conf}$ also shows that even at very high temperatures (close to T_m) entropy might not be used as a criterion of single phase stability of HEAs. We develop an analogy between CSS and glassy phases to develop a novel definition of the order-disorder transition in CSS through a singularity in the CSS configurational entropy. In this way, the order-disorder CSS transition temperature T_{OD} was estimated for several alloys and was shown to behave relatively similar to VEC, a commonly used HEA stability predictor. It is important to remark that computing T_{OD} requires special computational methods and a correct choice of the interatomic potential. However, the definition and relevance of T_{OD} to CSS formability provides a novel physical viewpoint for understanding of CSS thermodynamics.

In addition, we evince a kinetic and thermodynamic connection in the glass state and we hypothesize that it holds, analogously, in CSS states, with respect to kinetic migration. Motivated by glass phenomenology, such a relation for CSS allows us to explain diffusion and phase stability in terms of $S_{\rm conf}$ and T_{OD}. Our results also lead us to conclude that $S^g_{\rm conf}$ might not be considered as the only quantity to account for the critical slowing down in the supercooled regime.

The RS method employed in this work has been shown to be very efficient to calculate the configurational entropy in both the crystal and glass states, with results that are in good

agreement with experimental findings of these HEAs. Given the lack of simulation studies of Co-Cr-Fe-Ni-Mn HEAs in their glass state, our work paves the way to deepen the theoretical understanding of the order-disorder transition in solid solutions, as well as the glass transition in metallic glasses, mainly considering that they may be excellent candidates to explore ultrastable HEAs or/and metallic glasses [76], and the validity of the Adam-Gibbs equation as well as possible generalizations [77,78]. Further mechanical, dynamical, and thermal analysis of the CSS and glass states obtained here will be performed in a future work.

ACKNOWLEDGMENTS

This research was funded by the European Union Horizon 2020 research and innovation program under Grant Agreement No. 857470 and from the European Regional Development Fund via the Foundation for Polish Science International Research Agenda PLUS program Grant No. MAB PLUS/2018/8. We acknowledge the computational resources provided by the High-Performance Cluster at the National Centre for Nuclear Research in Poland.

[1] C. Li, J. C. Li, M. Zhao, and Q. Jiang, J. Alloys Compd. **475**, 752 (2009).
[2] Z. Li, K. G. Pradeep, Y. Deng, D. Raabe, and C. C. Tasan, Nature (London) **534**, 227 (2016).
[3] C. Lin and H. L. Tsai, Intermetallics **19**, 288 (2011).
[4] D. Ma, B. Grabowski, F. Körmann, J. Neugebauer, and D. Raabe, Acta Mater. **100**, 90 (2015).
[5] L. J. Santodonato, P. K. Liaw, R. R. Unocic, H. Bei, and J. R. Morris, Nat. Commun. **9**, 4520 (2018).
[6] Y. Zhang, G. L. Chen, and C. L. Gan, J. ASTM Int. **7**, 102819 (2010).
[7] Y. Zhang, T. Zuo, Z. Tang, M. C. Gao, K. A. Dahmen, P. K. Liaw, and Z. P. Lu, Prog. Mater. Sci. **61**, 1 (2014).
[8] A. Esfandiarpour, S. Papanikolaou, and M. Alava, Phys. Rev. Res. **4**, L022043 (2022).
[9] J. Yeh, S. Chen, S. Lin, J. Gan, T. Chin, T. Shun, C. Tsau, and S. Chang, Adv. Eng. Mater. **6**, 299 (2004).
[10] P. Huang, J. Yeh, T. Shun, and S. Chen, Adv. Eng. Mater. **6**, 74 (2004).
[11] O. Senkov, J. Scott, S. Senkova, D. Miracle, and C. Woodward, J. Alloys Compd. **509**, 6043 (2011).
[12] B. Cantor, I. Chang, P. Knight, and A. Vincent, Mater. Sci. Eng., A **375-377**, 213 (2004).
[13] J.-W. Yeh, S.-J. Lin, T.-S. Chin, J.-Y. Gan, S.-K. Chen, T.-T. Shun, C.-H. Tsau, and S.-Y. Chou, Metall. Mater. Trans. A **35**, 2533 (2004).
[14] F. Otto, Y. Yang, H. Bei, and E. George, Acta Mater. **61**, 2628 (2013).
[15] M. J. Yao, K. G. Pradeep, C. C. Tasan, and D. Raabe, Scr. Mater. **72-73**, 5 (2014).
[16] M.-R. Chen, S.-J. Lin, J.-W. Yeh, S.-K. Chen, Y.-S. Huang, and C.-P. Tu, Mater. Trans. **47**, 1395 (2006).
[17] N. Jones, R. Izzo, P. Mignanelli, K. Christofidou, and H. Stone, Intermetallics **71**, 43 (2016).
[18] X. Xu, P. Liu, S. Guo, A. Hirata, T. Fujita, T. Nieh, C. Liu, and M. Chen, Acta Mater. **84**, 145 (2015).
[19] F. Otto, A. Dlouhy, K. G. Pradeep, M. Kuběnová, D. Raabe, G. Eggeler, and E. P. George, Acta Mater. **112**, 40 (2016).
[20] M. Laurent-Brocq, A. Akhatova, L. Perrière, S. Chebini, X. Sauvage, E. Leroy, and Y. Champion, Acta Mater. **88**, 355 (2015).
[21] Q. F. He, Y. Ye, and Y. Yang, J. Appl. Phys. **120**, 154902 (2016).
[22] Q.-J. Li, H. Sheng, and E. Ma, Nat. Commun. **10**, 3563 (2019).
[23] W. Klement, R. H. Willens, and P. Duwez, Nature (London) **187**, 869 (1960).
[24] G. Kumar, H. X. Tang, and J. Schroers, Nature (London) **457**, 868 (2009).
[25] G. Kumar, A. Desai, and J. Schroers, Adv. Mater. **23**, 461 (2011).
[26] D. L. Henann, V. Srivastava, H. K. Taylor, M. R. Hale, D. E. Hardt, and L. Anand, J. Micromech. Microeng. **19**, 115030 (2009).
[27] P. G. Debenedetti and F. H. Stillinger, Nature (London) **410**, 259 (2001).
[28] G. Adam and J. Gibbs, J. Chem. Phys. **43**, 139 (1965).
[29] S. Sastry, Nature (London) **409**, 164 (2001).
[30] C.-S. Lee, M. Lulli, L.-H. Zhang, H.-Y. Deng, and C.-H. Lam, Phys. Rev. Lett. **125**, 265703 (2020).
[31] L. Berthier and G. Biroli, Rev. Mod. Phys. **83**, 587 (2011).
[32] M. Ozawa, C. Scalliet, A. Ninarello, and L. Berthier, J. Chem. Phys. **151**, 084504 (2019).
[33] P. H. Handle and F. Sciortino, Mol. Phys. **116**, 3366 (2018).
[34] A. Gali and E. P. George, Intermetallics **39**, 74 (2013).
[35] F. Otto, A. Dlouhy, C. Somsen, H. Bei, G. Eggeler, and E. George, Acta Mater. **61**, 5743 (2013).
[36] C. Zhu, Z. Lu, and T. Nieh, Acta Mater. **61**, 2993 (2013).
[37] M. W. Glasscott, A. D. Pendergast, S. Goines, A. R. Bishop, A. T. Hoang, C. Renault, and J. E. Dick, Nat. Commun. **10**, 2650 (2019).
[38] H. S. Oh, S. J. Kim, K. Odbadrakh, W. H. Ryu, K. N. Yoon, S. Mu, F. Körmann, Y. Ikeda, C. C. Tasan, D. Raabe, T. Egami, and E. S. Park, Nat. Commun. **10**, 2290 (2019).
[39] B.-J. Lee and M. I. Baskes, Phys. Rev. B **62**, 8564 (2000).
[40] W.-M. Choi, Y. H. Jo, S. S. Sohn, S. Lee, and B.-J. Lee, npj Comput. Mater. **4**, 1 (2018).
[41] S. Plimpton and B. Hendrickson, J. Comput. Chem. **17**, 326 (1996).
[42] G. J. Martyna, M. E. Tuckerman, D. J. Tobias, and M. L. Klein, Mol. Phys. **87**, 1117 (1996).
[43] G. J. Martyna, D. J. Tobias, and M. L. Klein, Constant pressure molecular dynamics algorithms, J. Chem. Phys. **101**, 4177 (1994).
[44] B. Sadigh, P. Erhart, A. Stukowski, A. Caro, E. Martinez, and L. Zepeda-Ruiz, Phys. Rev. B **85**, 184203 (2012).
[45] M. de Koning, A. Antonelli, and S. Yip, Phys. Rev. Lett. **83**, 3973 (1999).
[46] C. R. Miranda and A. Antonelli, J. Chem. Phys. **120**, 11672 (2004).
[47] M. de Koning, A. Antonelli, and S. Yip, J. Chem. Phys. **115**, 11025 (2001).

[48] F. Sciortino, W. Kob, and P. Tartaglia, Phys. Rev. Lett. **83**, 3214 (1999).
[49] W. Kauzmann, Chem. Rev. (Washington, DC, US) **43**, 219 (1948).
[50] D. Frenkel and A. J. C. Ladd, J. Chem. Phys. **81**, 3188 (1984).
[51] L. Berthier, M. Ozawa, and C. Scalliet, J. Chem. Phys. **150**, 160902 (2019).
[52] R. Paula Leite, R. Freitas, R. Azevedo, and M. de Koning, J. Chem. Phys. **145**, 194101 (2016).
[53] R. Paula Leite, P. A. Santos-Flórez, and M. de Koning, Phys. Rev. E **96**, 032115 (2017).
[54] R. Freitas, M. Asta, and M. de Koning, Comput. Mater. Sci. **112**, 333 (2016).
[55] M. Ozawa, G. Parisi, and L. Berthier, J. Chem. Phys. **149**, 154501 (2018).
[56] R. Paula Leite and M. de Koning, Comput. Mater. Sci. **159**, 316 (2019).
[57] O. Kubaschewski, C. B. Alcock, and P. Spencer, *Materials Thermochemistry*, revised (Pergamon Press Ltd., Oxford, 1993), p. 363.
[58] R. Alvarez-Donado, S. Cajahuaringa, and A. Antonelli, Phys. Rev. Mater. **3**, 085601 (2019).
[59] R. Alvarez-Donado and A. Antonelli, Phys. Rev. Res. **2**, 013202 (2020).
[60] Z. Wu, H. Bei, G. M. Pharr, and E. P. George, Acta Mater. **81**, 428 (2014).
[61] S. Haas, M. Mosbacher, O. N. Senkov, M. Feuerbacher, J. Freudenberger, S. Gezgin, R. Völkl, and U. Glatzel, Entropy **20**, 654 (2018).
[62] A. Banerjee, S. Sengupta, S. Sastry, and S. M. Bhattacharyya, Phys. Rev. Lett. **113**, 225701 (2014).
[63] R. Richert and C. Angell, J. Chem. Phys. **108**, 9016 (1998).
[64] M. C. Gao, C. Zhang, P. Gao, F. Zhang, L. Z. Ouyang, M. Widom, and J. Hawk, Curr. Opin. Solid State Mater. Sci. **21**, 238 (2017).
[65] A. Fernández-Caballero, M. Fedorov, J. S. Wróbel, P. M. Mummery, and D. Nguyen-Manh, Entropy **21**, 68 (2019).
[66] M. Fedorov, J. S. Wróbel, A. Fernández-Caballero, K. J. Kurzydłowski, and D. Nguyen-Manh, Phys. Rev. B **101**, 174416 (2020).
[67] P. Richet, Geochim. Cosmochim. Acta **48**, 471 (1984).
[68] P. Richet, J. Non-Cryst. Solids **355**, 628 (2009).
[69] Q. Liao and L. Berthier, Phys. Rev. X **9**, 011049 (2019).
[70] L. Berthier, Phys. Rev. Lett. **127**, 088002 (2021).
[71] K. Y. Tsai, M. H. Tsai, and J. W. Yeh, Acta Mater. **61**, 4887 (2013).
[72] W. Chen and L. Zhang, J. Phase Equilib. Diffus. **38**, 457 (2017).
[73] M. Vaidya, S. Trubel, B. S. Murty, G. Wilde, and S. V. Divinski, J. Alloys Compd. **688**, 994 (2016).
[74] Y.-Z. Wang and Y.-J. Wang, Acta Mater. **224**, 117527 (2022).
[75] L. J. Santodonato, Y. Zhang, M. Feygenson, C. M. Parish, M. C. Gao, R. J. K. Weber, J. C. Neuefeind, Z. Tang, and P. K. Liaw, Nat. Commun. **6**, 5964 (2015).
[76] A. Ninarello, L. Berthier, and D. Coslovich, Phys. Rev. X **7**, 021039 (2017).
[77] T. R. Kirkpatrick, D. Thirumalai, and P. G. Wolynes, Phys. Rev. A **40**, 1045 (1989).
[78] V. Lubchenko and P. G. Wolynes, Annu. Rev. Phys. Chem. **58**, 235 (2007).